QUANTUM PARTICLE SWARM OPTIMIZATION APPLIED TO AUTOMATED CRACK PATTERN ASSESSMENT OF BACKSCATTERED ELECTRON IMAGE IN CEMENTITIOUS SYSTEMS

Eduardo Vieira Queiroga[1*], Lucídio dos Anjos Formiga Cabral[1], Andressa Porto Vieira[2], Marçal Rosa Flores Lima Filho[2], Kelly Cristiane Gomes[2], Sandro Marden Torres[2]

[1]Centro de Informática - Universidade Federal da Paraíba - UFPB

[2]Centro de Tecnologia - Universidade Federal da Paraíba – UFPB

Paraíba, PB, BRAZIL

Abstract

Alkali-Aggregate Reaction (AAR) is a concrete pathology that is mostly acknowledged by its map cracking pattern look at macro-level. At micro-level, it is also well established that the formation of AAR gels can be responsible for the shaping of cracks within aggregates and pores. This paper presents an automatic crack detection in cementitious systems affected by mechanisms of cracking. The assessment was made via Scanning Electron Microscopy by using Back-scattered Electron Imaging (BEI) mode (Quanta 450 FEI). On this image mode, the grey level can be associated to particular features of hydration as well as pores and cracks in cementitious systems. The hydrated cement samples were sliced, ground and polished down to a quarter of microns prior to vacuum gold-sputtering process. The original grayscale scanned image of each BEI was analyzed by using morphological image processing techniques and threshold operations. A multilevel thresholding operation was performed by using the *Quantum Particle Swarm Optimization* (QPSO) approach to Otsu's criteria. The preliminary results point out to good performance and show a rough calculation for the area fraction phases, as well as the automatic crack measurements of the resulting binary image by graph algorithms.

Keywords: Concrete, Backscattered Electron Image Analysis, Optimization, Crack Detection.

1 INTRODUCTION

Alkali Aggregate Reaction (AAR) is a concrete pathology that occurs between some aggregate types and the alkalis in the pore solution of concrete, forming a gel that can be responsible for the shaping of cracks within aggregates and pores, reducing the durability and mechanical properties of concrete. The microstructural analysis for quantifying the cracks and investigate its relationship with other aspects of concrete (e.g. aggregate distribution and hydrated cement content), can be important for the conception of criteria for diagnosis and assessment of the degree of reaction.

The analysis of polished concrete samples by Backscattered Electron Image (BEI) has shown a great potential [1]. Image analysis procedures for characterization of concrete phases has been proposed for quantifying anhydrous and hydrated cement content [2,3,4], porosity [5,6,7] and aggregate [8]. In the literature the use of multilevel thresholding for BEI segmentation has been little explored, usually applying simple thresholding techniques separately.

The use of swarm intelligence optimization algorithms for image segmentation tasks have been extensively studied [9]. Some works [10,11,12] proposed to optimize the multilevel Otsu's method of the maximum between-classes variance. These techniques can be an alternative to the exhaustive searching methods that are infeasible in some applications due to the computational cost involved.

As a later step to the segmentation phase, the crack modeling in graph structures has been recently explored [13,14], enabling the proposition of methods for features extraction with great capacity to deal with connectivity.

In this paper, the *Quantum Particle Swarm Optimization* (QPSO) is applied to BEI segmentation of cement paste specimens as preliminary step to the crack detection, besides allowing the area fraction calculation of phases. We apply morphological operations as a preprocessing step to adjust the crack binary image. We also propose the use of graph algorithms for pore filtering and automatic extraction of the length and width of the cracks. In section 2, the materials and methods are described.

* Correspondence to: eduardo.queiroga@ci.ufpb.br

The automated process of image analysis is explained in section 3. Preliminary results are shown in section 4 followed by the final remarks.

2 MATERIALS AND METHODS

2.1 Materials and mix designs

Samples were cast using early strength development Portland cement and two water to binder ratio (0.33 and 0.44 by mass) as presented in Table 1. Two sets of cement pastes were mixed with and without an ultrafine ground redbrick waste pozzolan (15,000 cm^2/g Blaine) replacing cement (20% by mass). Fractured samples were lapped and polished down to 1/4 micron prior to testing. The samples were analyzed by Scanning Electron Microscopy (Backscattered Electron Imaging Mode). Test ages were 1, 3 and 7 days.

TABLE 1: Composition of mixtures used in the microstructural analysis.

Mixture	Water/binder ratio (w/b)	Cement	Pozzolan
M33	0.33	1	0
M44	0.44	1	0
M33PZ	0.33	0.8	0.2
M44PZ	0.44	0.8	0.2

2.2 Methods for assessment and analysis

The hydrated cement samples were sliced, ground and polished down to a quarter of microns prior to vacuum gold-sputtering process. The assessment by microstructural characterization was made via Scanning Electron Microscopy by using Backscattered Electron Image (BEI) mode (Quanta 450 FEI). The SEM was used with an acceleration voltage of 20 kV and magnification of 500x. All image analysis procedures will be described in detail in the next section.

3 ANALYSIS IMAGE PROCEDURES

The histogram of a specimen, as shown in Figure 1, has peaks that indicates some phases with the exception of pores. Finding suitable thresholds can provide a good segmentation and it depends of the chosen method. The Otsu's method qualifies a thresholding by maximum inter-class variance, as detailed in Appendix I. The flow diagram in Figure 2 shows the steps associated to the process that was implemented and executed in MATLAB R2012a platform using the image processing toolbox. The first step consists on the QPSO multilevel thresholding (see section 3.1). Next, morphological operations are applied to crack binary image for adjustment and recovery of cracks. Finally, the cracks are modeled with a graph to filter the pores and extracting the attributes of interest.

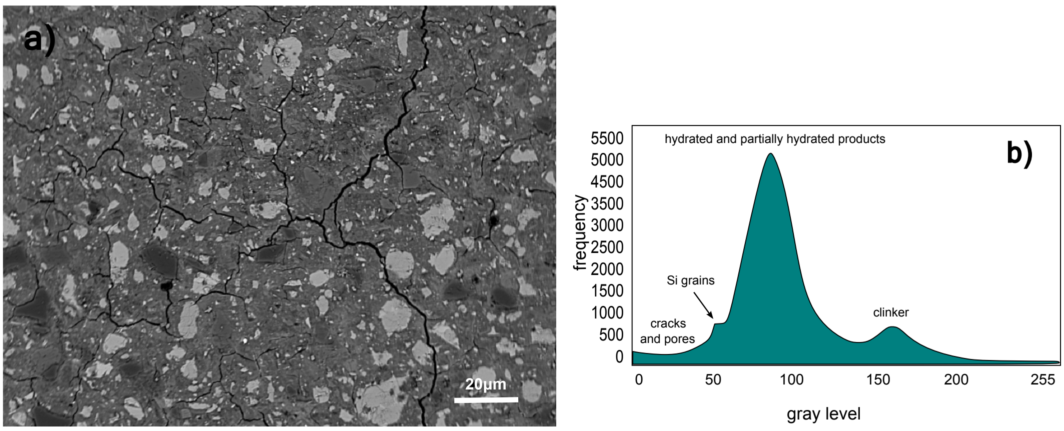

FIGURE 1: a) BEI of the specimen M33PZ observed with one day of age. b) Histogram with peaks associated to phases.

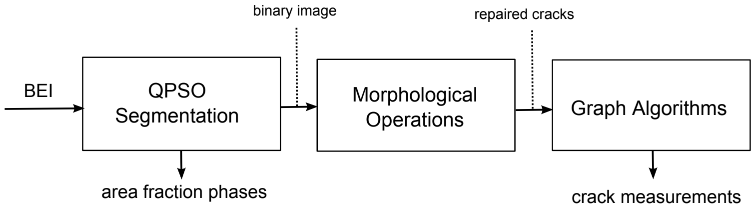

FIGURE 2: Flow chart of the crack detection process.

3.1 Quantum Particle Swarm Optimization applied to BEI segmentation

Particle Swarm Optimization (PSO) is a stochastic optimization method proposed by Kennedy and Eberhart [15] that solves a problem by iteratively move a set of particles, called swarm, around in the multidimensional space according to equations over the particle's position and velocity. The algorithm was motivated by social behavior of organisms such as birds while searching for food. For each new particle position, a different problem solution is generated. This solution is evaluated by an *objective function* or *fitness,* which must be optimized (minimized or maximized) and provides a quantitative value of the particle in question. The particles determines their positions and velocities through the search space according to the best fitness throughout its history or personal best (*pbest*) and global best position (*gbest*) obtained by swarm, as shown in equation (1) and (2). $V_{i,j}^{t+1}$ represents the velocity vector for *i*-th particle in the dimension j in the iteration t+1; w is an inertial weight, c_1 and c_2 are acceleration constants and $r_{1j}, r_{2j} \in [0,1]$ are random values uniformly distributed.

$$V_{i,j}^{t+1} = w \times V_{i,j}^{t} + c_1 \times r_{1j} \times \left(pbest_{i,j} - X_{i,j}^{t}\right) + c_2 \times r_{2j} \times \left(gbest_{i,j} - X_{i,j}^{t}\right) \quad (1)$$
$$X_{i,j}^{t+1} = X_{i,j}^{t} + V_{i,j}^{t+1} \quad (2)$$

The PSO algorithm pseudocode has the following steps:
Step 1: Initialize swarm of particles with random positions, calculate fitness of each particle (initial *pbest)* and find the initial *gbest*;
Step 2: Calculate velocity vectors and positions using equations (3) and (4);
Step 3: Update, when improvement occurs, *pbest* and *gbest*;
Step 4: If the termination criteria is found, return to *gbest* solution. Otherwise, go to *Step 2.*

In many applications, quantum-behaved PSO (QPSO) algorithms can be more efficient than conventional PSO. The quantum system is not a simple linear system, but a complex nonlinear system, and follows the superposition principle of states [12]. In QPSO, replacing the equations (1) and (2) by equations (3), (4) and (5) to control the movements of the particles by sampling the wave function in a quantum system.

$$mbest = \frac{1}{M}\sum_{i=1}^{M} p_i = \left(\frac{1}{M}\sum_{i=1}^{M} p_{i1}, \frac{1}{M}\sum_{i=1}^{M} p_{i2}, \dots, \frac{1}{M}\sum_{i=1}^{M} p_{id}\right) \quad (3)$$
$$A_i = \varphi \times p_i(t) + (1 - \varphi) \times p_g \quad (4)$$
$$x_i(t+1) = A_i \pm \alpha \times |mbest - x_i(t)| \times \ln(\tfrac{1}{u}) \quad (5)$$

where *mbest* (3) is the mean position of the personal bests in the swarm with M particles and d dimensions. A_i (6) is the local attractor of the *i*-th particle, which combines information from personal best and global best, weighted by $\varphi \in [0,1]$, random value uniformly distributed. $x_i(t+1)$ is the new particle position , where is fixed the creativity coefficient and u $\in [0,1]$ random value uniformly distributed. Several particles can be generated and cooperative approaches can be used to find the best move, as explored in [12,17].

For BEI segmentation, each particle in QPSO retains a set of *k* thresholds (particles moves in *k*-dimensional space) and the fitness value is the multilevel Otsu's method. A simple modification in the objective function may be carried out by weighing the class variance terms with $\lambda = \{\lambda_1, \lambda_2, \dots, \lambda_k\}$, as shown in equation (6). This adaptation can generates interesting results and provides a parametrization for different application contexts.

$$f(t) = \lambda_1 \times w_1 \times (\mu_1 - \mu) + \lambda_2 \times w_2 \times (\mu_2 - \mu) + \cdots \lambda_k \times w_k \times (\mu_k - \mu) \quad (6)$$

3.2 Morphological operations

On the morphological operators, the effect is determined by a structuring element that consists of a rectangular grid with small dimensions and specified pattern. The structuring element probes the binary image by positioning its origin, often the matrix center, with each pixel and verifies if it hits, fills or fills other active pixels (equals to one), depending on the operator's choice. These operations are useful to correct binary images. In the case studied, for solving some discontinuities in cracks, a closing operation (dilation followed by erosion operation) was performed with 4x4 square and 3x3 diamond structuring element.

3.3 Crack measurements by graph algorithms

A graph is a mathematical modeling tool that consists of nodes and edges representing entities and relationships, respectively. We can model a crack as a graph G from its binary image (Figure 3 (a)), This is made by creating a node for each pixel that maps the crack and edges linking orthogonal and diagonal nodes, as shown in Figure 3 (b). Using a depth-first search algorithm [18], we can easily separate the cracks by exploring the connectivity and eliminate the low cardinality components (see Figure 3 (b)). In Figure 3 (c) we can observe a reduction graph generated by Kruskal's algorithm [19], which reduces the computational costs of subsequent procedures. Then pruning operation is performed to obtain the graph skeleton over which is calculated the diameter of each connected component of the graph, which refers to the length of the underlying cracks.

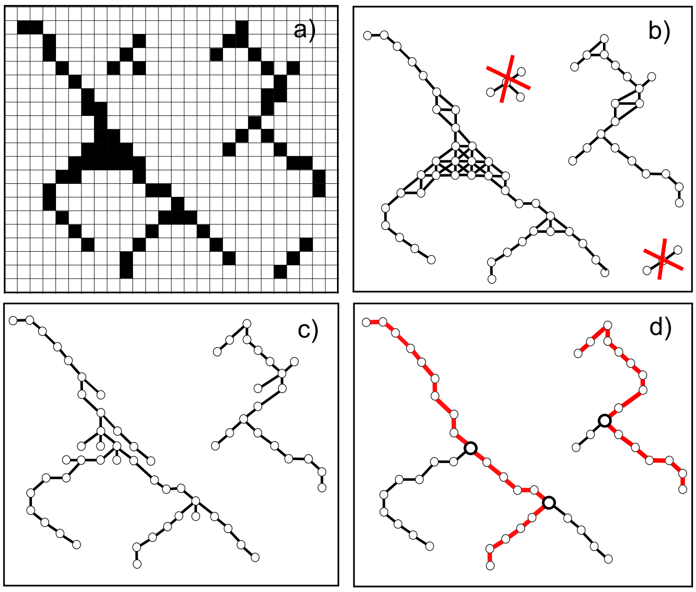

FIGURE 3: a) Synthetic binary image. b) Underlying graph G. c) G filtered and processed by Kruskal's algorithm. d) Skeleton graph obtained by pruning operation.

A pore filter can be designed to eliminate connected components by high cardinality-diameter ratio, which removes rounded shape objects if the inequality (7) is satisfied. Good results were obtained for $t_p = 0.25$.

$$\frac{|G_c|}{d(G_c)} > t_p \qquad (7)$$

The figure 4 shows the full process for crack detection, starting with the original BEI in Figure 4(a). Next, in Figure 4 (b) we have a binary crack image that is processed by dilation and erosion morphological operations (see Figure 4(c) and 4(d)). Finally, the resulting image is filtered by graph algorithms that eliminates small connected components (see Figure 4(e)) and pores (see Figure 4(f)).

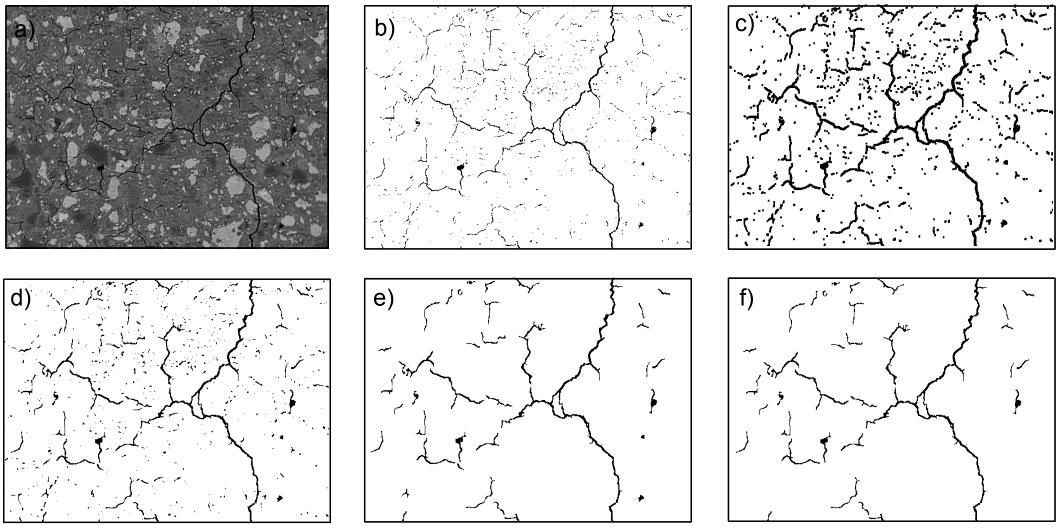

FIGURE 4: Crack detection process. a) Original BEI. b) Crack binary image. c) Result of the dilatation operation. d) Result of the erosion operation e) Graph filtering for small components. f) Graph pore filtering.

4 PRELIMINARY RESULTS

As already discussed, weighing the terms of the Otsu's function can improve the segmentation results, as shown in Figure 5. In Figure 5(a) and 5(b) we have the result for two thresholds with original and weighted (by $\lambda_1 = 0.93$) criteria, respectively. There is a clear difference between the segmentations, since the cracks and pores were better separated from the intermediate phase. In Figure 5(c) and 5(d), for three thresholds and $\lambda_1 = 0.95$, $\lambda_2 = 0.96$, the Si grains were segmented successfully, as well as pores and cracks.

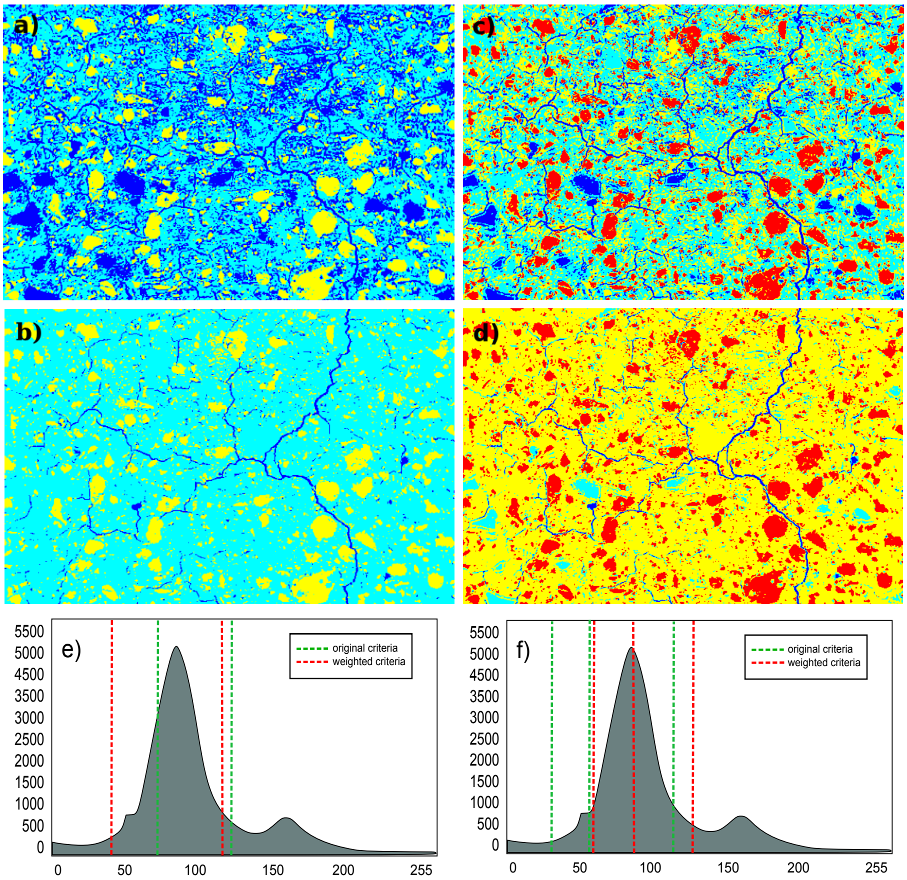

FIGURE 5: Effect of the modification proposed in Otsu's method. a)-c) Results for the original method. b)-d) Results for the weighted method. e)-f) Comparison of the thresholds in histogram.

More results for crack detection are shown in Figure 6 for specimens M33 and M33PZ observed in one and seven days, respectively. In Figure 6(a) and 6(d) we have the original BEI with its segmentation in Figure 6(b) and 6(e). In Figure 6(c) and 6(f) the cracks detected are presented.

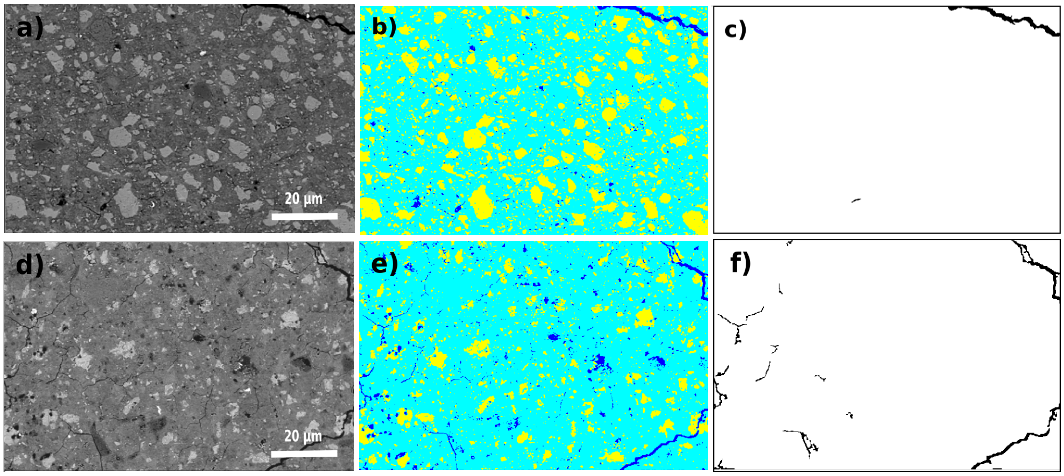

FIGURE 6: a)-d) BEI for M33 and M33PZ samples with one and seven days, respectively. b)-d) Segmentation results for two thresholds. c)-f) Final result of crack detection for both specimens.

In Table 2, some crack measurements such as the number of cracks, maximum length and width, are reported for the three BEI illustrated in this paper. The length was calculated by graph diameter algorithm. The widths were obtained by a simple procedure based on region growing methods that seeks the maximum neighborhood quadratic matrix in the crack for each internal pixel. In Table 3 the area fraction of the phases are reported for twelve specimens segmented by QPSO with two thresholds.

TABLE 2: Crack measurements obtained by graph algorithms.

Specimen	Age (days)	#Cracks	Maximum length (px)	Maximum width (px)
M33	1	2	200	7
M33PZ	1	35	421	7
M33PZ	7	17	142	5

TABLE 3: Area fraction of the phases calculated by segmentation results.

Specimen	Age (days)	Pores (%)	Crack (%)	Si grains + hydrated products (%)	Clinker (%)
M33	1	0.51	0.61	76.78	22.09
M33	3	3.54	0.27	70.83	25.36
M33	7	0.47	0.00	82.11	17.42
M44	1	0.20	0.90	83.03	15.87
M44	3	2.23	0.00	85.41	12.35
M44	7	0.84	0.22	84.30	14.63
M33PZ	1	1.03	1.65	80.72	16.59
M33PZ	3	0.39	0.24	85.15	14.18

Specimen	Age (days)	Pores (%)	Crack (%)	Si grains + hydrated products (%)	Clinker (%)
M33PZ	7	2.15	1.02	85.56	11.26
M44PZ	1	0.77	0.22	81.63	17.38
M44PZ	3	2.97	0.53	73.91	22.59
M44PZ	7	1.46	0.98	88.77	8.80

5 FINAL REMARKS

In this paper we proposed to quantify the phases of the cement paste by multilevel thresholding with the Quantum Particle Swarm Optimization (QPSO) algorithm that optimizes Otsu's criteria. We have also proposed modeling the resulting binary image as a graph to extract features of interest. The procedures can easily adapt to new specimen settings with necessary adjustments to the existing parameters. As future work, new features related to crack branching can be extracted for map cracking and machine learning models (e.g. Artificial Neural Networks) can be explored for damage prognosis.

.

ACKNOWLEDGMENTS

The authors acknowledge the help of TECNOMAT-UFPB laboratory support. Some of the authors would like to thank the Brazilian institution CHESF-PE for the financial support.

REFERENCES

[1] Scrivener, K. L. (2004): Backscattered electron imaging of cementitious microstructures: understanding and quantification. *Cement and Concrete Composites*, *26*(8), 935-945.

[2] Mouret, M., E. Ringot, and A. Bascoul. "Image analysis: a tool for the characterisation of hydration of cement in concrete–metrological aspects of magnification on measurement." *Cement and Concrete Composites* 23.2 (2001): 201-206.

[3] Igarashi, Shin-ichi, M. Kawamura, and A. Watanabe. "Analysis of cement pastes and mortars by a combination of backscatter-based SEM image analysis and calculations based on the Powers model." *Cement and Concrete Composites* 26.8 (2004): 977-985.

[4] Oueslati, O., and J. Duchesne. "Resistance of blended cement pastes subjected to organic acids: Quantification of anhydrous and hydrated phases." *Cement and Concrete Composites* 45 (2014): 89-101.

[5] Lange, D. A., Jennings, H. M., & Shah, S. P. (1994): Image analysis techniques for characterization of pore structure of cement-based materials.*Cement and Concrete Research*, *24*(5), 841-853.

[6] Igarashi, Shin-ichi, Akio Watanabe, and Mitsunori Kawamura. "Evaluation of capillary pore size characteristics in high-strength concrete at early ages."*Cement and Concrete Research* 35.3 (2005): 513-519.

[7] Wong, H. S., M. K. Head, and N. R. Buenfeld. "Pore segmentation of cement-based materials from backscattered electron images." *Cement and Concrete Research* 36.6 (2006): 1083-1090.

[8] Yang, R., and N. R. Buenfeld. "Binary segmentation of aggregate in SEM image analysis of concrete." *Cement and Concrete Research* 31.3 (2001): 437-441.

[9] Kaur, A., & Singh, M. D. (2012): An Overview of PSO-Based Approaches in Image Segmentation. *International Journal of Engineering and Technology*,*2*(8).

[10] Duraisamy, S. P., & Kayalvizhi, R. (2010): A new multilevel thresholding method using swarm intelligence algorithm for image segmentation. *Journal of Intelligent Learning Systems and Applications*, *2*(03), 126.

[11] Misra, D., Bose, I., De Chandra, U., & Pradhan, B. (2014): A multilevel image thresholding using particle swarm optimization. *International Journal of Engineering and Technology*, *6*(2), 698-705.

[12] Li, Y., Jiao, L., Shang, R., & Stolkin, R. (2015): Dynamic-context cooperative quantum-behaved particle swarm optimization based on multilevel thresholding applied to medical image segmentation. *Information Sciences*,*294*, 408-422.
[13] Zou, Q., Cao, Y., Li, Q., Mao, Q., & Wang, S. (2012): CrackTree: Automatic crack detection from pavement images. *Pattern Recognition Letters*, *33*(3), 227-238.
[14] Luo, Z., Zhu, Z., Ruan, H., & Shi, C. (2015): Extraction of microcracks in rock images based on heuristic graph searching and application. *Computers & Geosciences*, *85*, 22-35.
[15] Eberhart, R. C., & Kennedy, J. (1995, October): A new optimizer using particle swarm theory. In *Proceedings of the sixth international symposium on micro machine and human science* (Vol. 1, pp. 39-43).
[16] Li, Y., Xiang, R., Jiao, L., & Liu, R. (2012): An improved cooperative quantum-behaved particle swarm optimization. *Soft Computing*, *16*(6), 1061-1069.
[17] Tarjan, R. (1972): Depth-first search and linear graph algorithms. *SIAM journal on computing*, *1*(2), 146-160.
[18] Kruskal, J. B. (1956): On the shortest spanning subtree of a graph and the traveling salesman problem. *Proceedings of the American Mathematical society*, *7*(1), 48-50.

Appendix I

For the set of segments $S = \{S_1, S_2, \dots, S_k\}$ and the set of thresholds $T = \{t_1, t_2, \dots, t_k\}$ we have $S_1 = [0, \dots, t_1 - 1], S_2 = [t_1, \dots, t_2 - 1], \dots, S_1 = [t_k, \dots, L - 1]$ for an image with 0 up to L-1 gray level. The probability for each segment is given by $w_1 = \sum_{i=0}^{t_1-1} p_i, w_2 = \sum_{i=t_1}^{t_2-1} p_i, \dots, w_k = \sum_{i=t_k}^{L-1} p_i$, where $p_i = \frac{h(i)}{N}$ for h(*i*) as level frequency of *i* in histogram with N pixels. The mean for each segment is $\mu_1 = \sum_{i=0}^{t_1-1} \frac{i \times h(i)}{w_1 \times N}$, $\mu_2 = \sum_{i=t_1}^{t_2-1} \frac{i \times h(i)}{w_2 \times N}, \dots,$ $\mu_k = \sum_{i=t_k}^{L-1} \frac{i \times h(i)}{w_k \times N}$ and the total mean is equals to $\mu = w_1 \times \mu_1 + w_2 \times \mu_2 + \dots + w_k \times \mu_k$. The Otsu's multilevel criteria seeks the thresholds that maximizes the inter-class variance for optimizing the function (12) as shown in equation (13)

$$f(T) = w_1 \times (\mu_1 - \mu) + w_2 \times (\mu_2 - \mu) + \cdots + w_k \times (\mu_k - \mu) \tag{12}$$

$$(t_1^*, t_2^*, \dots, t_k^*) = \arg \max_{0 \le t_1 \le t_2 \le \cdots \le t_k \ll 1} f(T) \tag{13}$$